IEEE Access
Multidisciplinary : Rapid Review : Open Access Journal

Received September 24, 2021, accepted October 19, 2021, date of publication October 22, 2021, date of current version October 29, 2021.

Digital Object Identifier 10.1109/ACCESS.2021.3122160

An IMUs-Based Extended Kalman Filter to Estimate Gait Lower Limb Sagittal Kinematics for the Control of Wearable Robotic Devices

JULIO S. LORA-MILLAN [1], ANDRES F. HIDALGO [2], AND EDUARDO ROCON [1], (Member, IEEE)
[1] Centro de Automática y Robótica, Consejo Superior de Investigaciones Científicas–Universidad Politécnica de Madrid (CSIC-UPM), 28040 Madrid, Spain
[2] Advanced Robotics, Istituto Italiano di Tecnologia, 16163 Genova, Italy

Corresponding author: Eduardo Rocon (e.rocon@csic.es)

This work was supported in part by the Spanish Ministry of Science and Innovation through the Project Discover2Walk under Grant PID2019-105110RB-C31, and in part by the Programas de Actividades I+D en la Comunidad de Madrid and Structural Funds of the EU (RoboCity) under Grant S2018/NMT-4331. The work of Julio S. Lora-Millan was supported by the Ministry of Universities of the Government of Spain through the Training Program for Academic Staff Fellowship under Grant FPU16/01313.

This work involved human subjects or animals in its research. Approval of all ethical and experimental procedures and protocols was granted by the Local Ethics Committee (CSIC's Ethics Committee) under Approval No. 034/2020, and performed in line with the Declaration of Helsinki.

ABSTRACT Inertial sensors have gained relevance as wearable sensors to acquire the kinematics of human limbs through fusion sensor algorithms and biomechanical models. However, there are some limitations to the use of Inertial Measurement Units in the control of wearable robotic devices: 1) Some approaches use magnetometer readings to estimate the orientation of the sensor, and, as a result, they are prone to errors due to electromagnetic interferences; 2) Biomechanical model-based approaches require complex and time-consuming calibration procedures. In order to address these issues, this paper proposes an Extended Kalman Filter to estimate sagittal lower limb kinematics during gait, based on gyroscopes and accelerometers and without requiring any calibration or sensor alignment process. As magnetometer measurements are not involved, this method is not affected by electromagnetic disturbances. Our approach calculates the knee rotation axis in real-time, and it estimates hip and ankle sagittal axes considering that the movements in that plane occur around parallel axes. We carried out an experimental validation with eight healthy subjects walking on a treadmill at different velocities. We obtained waveform RMS errors about 3.8°, 3.6°, and 4.8° for hip, knee, and ankle in the sagittal plane. We also assessed the performance of this method as a tool for controlling lower-limb robotic exoskeletons by detecting gait events or estimating the phase and frequency of the gait in real-time through an Adaptive Frequency Oscillator. The average RMS delay in the detection of gait events was lower than 60 ms, and the RMSE in the estimation of the gait phase was about 3% of the gait cycle. We conclude that the described method could be used as a controller for wearable robotic devices.

INDEX TERMS Inertial sensor, extended Kalman filter, lower-limb kinematics, robotic exoskeleton sensors.

I. INTRODUCTION

Inertial sensors have become valuable tools for acquiring human motion during complex functional tasks such as gait [1]. Inertial Measurement Units (IMUs) are composed of accelerometers, gyroscopes, and magnetometers that measure the information with respect to their own three-dimensional local coordinate systems [2]. Several fusion sensor algorithms were developed to use the information from these three kinds of sensors to estimate the IMU orientation with respect to a global coordinate system [3]. They are usually based on strap-down integration [4]–[6], nonlinear filtering techniques, such as Extended Kalman Filters [7], [8], or nonlinear numerical optimization [9], [10]. These algorithms assume that accelerometer readings are dominated by gravity at specific samples to correct vertical tilt [2], [6], [11], [12] or use magnetometer readings assuming magnetic field homogeneity to compensate for drift in the

The associate editor coordinating the review of this manuscript and approving it for publication was Dingguo Zhang.

This work is licensed under a Creative Commons Attribution-NonCommercial-NoDerivatives 4.0 License.
For more information, see https://creativecommons.org/licenses/by-nc-nd/4.0/

horizontal plane [6], [13]. In these last cases, magnetic disturbances may affect the performance of the orientation estimation [14], [15].

Although these techniques provide reliable information about the IMU orientation, estimating the orientation of a limb segment is not straightforward. Since there is no exact correspondence between the sensor's coordinate system and the human segment, it is necessary to deal with possible misalignments between them. To overcome this problem, some authors proposed the use of movements to calibrate a biomechanical model [11], [16], while others used prior knowledge like segment lengths or masses [5], [9], [10] or the position of the sensors with respect to the joint centers [8]. These calibrations are only valid while the sensors remain in the calibration position; thus, a new calibration is required if they change their position during an experiment.

As IMUs can directly measure a subject's movement, robotic wearable systems can use them to implement assistive strategies or rehabilitation therapies based on real human motion instead of using the robot's own movements (usually measured by encoders). Recently, robotic devices have shown promising results as therapeutic tools for gait rehabilitation of impaired patients [17], [18] as well as assistive devices to support their gait [19], [20]. Different approaches were followed to implement sensory systems in these devices [21], such as potentiometers or inertial sensors for measuring angles, torque sensors, or foot pressure sensors for acquiring ground reaction forces. Conversely, other authors opted for different approaches like using biosignals such as electroencephalography (EEG) [22] or electromyography (EMG) [23], [24], or new flexible sensors according to the soft-robotic paradigm [25]–[27].

The reduction in price and size of inertial sensors have spread their usage as sensory systems for robotic exoskeletons or active orthosis to acquire the kinematics of assisted [28]–[31] or unassisted [32], [33] lower limbs. However, these robotic applications imply severe drawbacks to the use of inertial sensors. In particular, IMUs are especially prone to magnetic disturbances from hospital environments [3] or elements of the experimental set-up (such as treadmill motors or exoskeleton actuators) [34]. On top of that, the calibration and alignment procedures required to use these systems are complex and time-consuming.

In this context, we developed an auto-adaptive algorithm based on inertial sensors that estimates the sagittal joint axes and the angular movements in human lower limbs during gait based on inertial sensors data. The overarching goal is to enable the application of this technology as a reliable input for the control of robotic wearable devices. The proposed algorithm addresses the three main limitations of this technology to be used in this field: (1) being not affected by magnetic disturbances, (2) easing calibration and donning procedures of the sensory system, and (3) being independent of the relative position between the IMU and the human limb.

To fulfill these requirements, our algorithm is based on the measurements from gyroscopes and accelerometers. As magnetometers are not involved, the system is unaffected by magnetic interferences. Besides, since the algorithm is able to estimate in real-time the coordinates of the axes, it does not require either previous calibration procedures or being aligned with human segments, being robust to possible sensor displacements during an experiment.

To validate the application of our method in the controller of a robotic exoskeleton, we evaluated its performance under two common control paradigms that are usual for these devices: 1) Detection of gait events for the definition of the device's action [35]–[39]; and 2) Estimation of the gait phase in real-time using an Adaptive Frequency Oscillator (AFO) [31], [40], [41]. Several authors have worked on gait event detection and gait segmentation [42], [43], and Prasanth *et al.* presented an extensive review of these methods in [44]; however, some of them have not been validated as controllers for robotic wearable devices, so they are out of the scope of this work.

In a nutshell, in this document, we propose an algorithm to estimate planar angular movements and their axes in real-time by fusing IMU signals. The algorithm is based on an Extended Kalman Filter, and it was used to estimate the hip, knee, and ankle movements in the sagittal plane. We also describe the experimental validation performed on healthy subjects in terms of errors, and, as application examples, we evaluated the use of this method as two typical controllers for robotic exoskeletons. Finally, we discuss the obtained results and confirm that our approach can be used as a tool for wearable robots' controllers as errors remained under the thresholds previously published in the literature.

II. MATERIALS AND METHODS

The algorithm presented in this document is an extension of our previous work [45], where we assumed that the knee is a perfect revolute joint, following the approach presented by Seel *et al.* [2]. Here, we also assume that hip, knee, and ankle sagittal movements occur around parallel axes. As a result, we can use the knee axis estimation to calculate the axis for hip flexion-extension and ankle dorsiflexion-plantarflexion. We also assume that the coordinates of these axes in the local coordinate systems of the IMUs are constant in time, although they are different between them, and their relative position may change over time (see Fig. 1, panels a and b).

A. PROBLEM FORMULATION

We assume that the rotation axis of a joint is invariant with respect to the local frame of the IMUs. Therefore, if $\mathbf{v}_D$ represents a unitary vector in the direction of the joint rotation axis in the local frame of the distal segment, and $\mathbf{v}_P$ represents the same joint axis vector in the local frame of the proximal segment, the joint angular velocity at the sample j, $\dot{\theta}_j$, can be computed as follows

$$\dot{\theta}_j = \boldsymbol{\omega}_{D_j}^T \mathbf{v}_D - \boldsymbol{\omega}_{P_j}^T \mathbf{v}_P \tag{1}$$

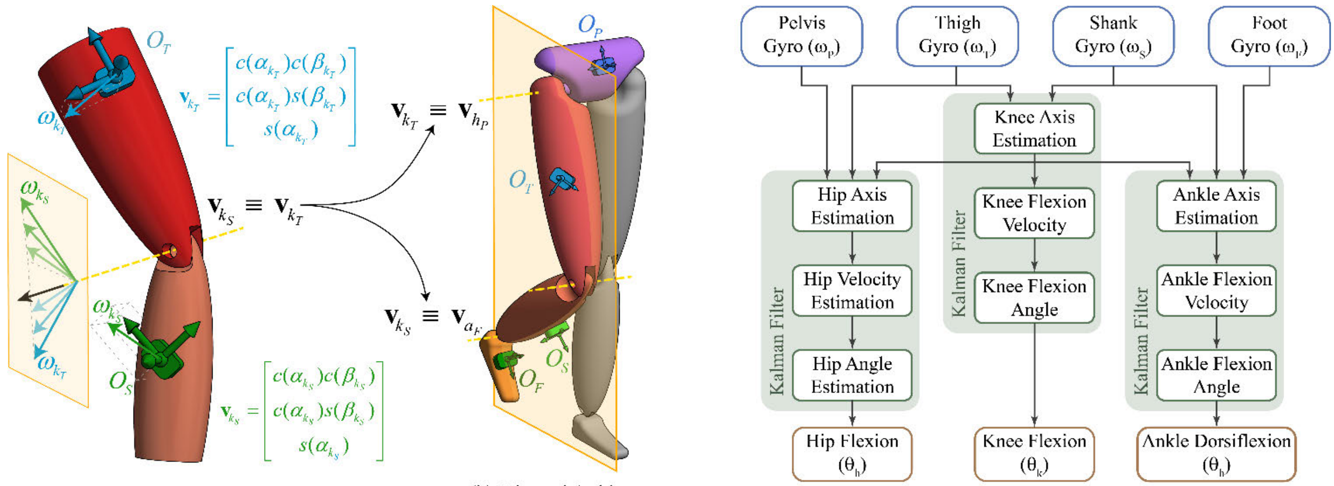

(a) Knee Joint Axis Estimation (b) Hip and Ankle Axis Estimation (c) Algorithm block diagram

FIGURE 1. Conceptual overview for the algorithm. In (a), we represent the calculus of the knee joint axis based on the knee angular velocities seen from the thigh (ω_{k_T}) and the shank (ω_{k_S}). In (b), we represent the hip flexo/extension axis and the ankle dorsiflexion/plantarflexion axis, which we assume are parallel to the knee axis. The origin of the local frames O_F and the unitary vectors for the joint axis v_{j_F} are also depicted. The subindex *j* indicates the joint involved (*h* for hip, *k* for knee, *a* for ankle), while the subindex *F* indicates the local frame from which the variable is seen (*P* for the pelvis, *T* for the thigh, *S* for the shank, *F* for foot). The unitary vectors for the joint axis are expressed in spheroidal coordinates where $c(\alpha)$ and $s(\alpha)$ represent the cosine and sine of the angle α. In (c), we include the block diagram of the algorithm and the information flow across it.

where $\boldsymbol{\omega}_{D_j}$ and $\boldsymbol{\omega}_{P_j}$ are the angular velocities of the distal (D) and proximal (P) segment of the joint measured by the corresponding IMUs at the sample j.

Taking into account the spheroidal coordinates of unitary vectors $\mathbf{v}_D$ and $\mathbf{v}_P$, we define the unknown vector $\bar{\mathbf{x}}$ as

$$\bar{\mathbf{x}} = \begin{bmatrix} \alpha_D & \beta_D & \alpha_P & \beta_P \end{bmatrix}^T \tag{2}$$

where the pairs (α, β) are the spheroidal coordinates of the joint axis seen form the distal (D) and proximal (P) sensor, respectively.

To calculate $\bar{\mathbf{x}}$, we use N sample times to define the error vector:

$$\mathbf{e}(\bar{\mathbf{x}}) = [e_1\ e_2\ \ldots\ e_j\ \ldots\ e_N]^T; \quad N \geq 4 \tag{3}$$

where the error $e(\bar{\mathbf{x}})_j$ at the sample j has the following expression

$$e(\bar{\mathbf{x}})_j = ||\boldsymbol{\omega}_{D_j} \times \mathbf{v}_D|| - ||\boldsymbol{\omega}_{P_j} \times \mathbf{v}_P|| \tag{4}$$

In this way, the unknown vector $\bar{\mathbf{x}}$ is iteratively computed using the Newton method as

$$\bar{\mathbf{x}}_{i+1} = \bar{\mathbf{x}}_i + \mathbf{G}(\bar{\mathbf{x}})_i^+ \mathbf{e}(\bar{\mathbf{x}})_i \tag{5}$$

where $\mathbf{G}(\bar{\mathbf{x}})_i^+$ is the pseudoinverse of the Jacobian matrix $\mathbf{G}(\bar{\mathbf{x}})$ at iteration i defined by

$$\mathbf{G}(\bar{\mathbf{x}})_i = \left.\frac{\partial \mathbf{e}(\bar{\mathbf{x}})}{\partial \bar{\mathbf{x}}}\right|_i \tag{6}$$

As shown by (6), the Jacobian matrix $\mathbf{G}(\bar{\mathbf{x}})_i$ is built from the error vector $\mathbf{e}(\bar{\mathbf{x}})_i$ that, at the same time, requires N measurements of the angular velocities $\boldsymbol{\omega}_{D_j}$ and $\boldsymbol{\omega}_{p_j}$ with $N \geq 4$.

At each sample time, the error vector $\mathbf{e}(\bar{\mathbf{x}})_j$ is updated with a new velocity measurement. Therefore, each iteration of (5) is performed with the $N = 10$ latest velocity measurements and with an updated Jacobian matrix $\mathbf{G}(\bar{\mathbf{x}})_i$. Because of the variation of these parameters for the sample j, equation (5) can be rewritten as:

$$\bar{\mathbf{x}}_{i+1} = \bar{\mathbf{x}}_i + \mathbf{G}(\bar{\mathbf{x}}, j)_i^+ \ \mathbf{e}(\bar{\mathbf{x}}, j)_i \tag{7}$$

B. MULTIJOINTPROBLEM EXTENSION

At this point, the process differs in function of the joint involved. Since we assumed that the knee joint is composed of a single axis, all the movement measured by the distal and proximal inertial sensors corresponds to the movement around this axis in the sagittal plane. Thereby, this axis is fully defined and can be iteratively calculated by solving (7) and considering the solution of the previous iteration $\bar{\mathbf{x}}_i$. This iterative problem is resolved by using the extended Kalman filter previously reported in [45] and summarized in the appendix of this document.

The unique-axis assumption cannot be maintained in hip and ankle joints as they allow movements in more planes. However, since IMUs in the thigh and the shank are also involved in the movements of hip and ankle joints respectively, and assuming that the rotation axes $\mathbf{v}$ of the sagittal movements are parallels, there is a correspondence between the coordinates of the rotation axes for different joints seen from the same IMU:

$$\mathbf{v}_{h_D} = \mathbf{v}_{k_P}; \quad \mathbf{v}_{a_P} = \mathbf{v}_{k_D} \tag{8}$$

where the subindexes indicate the joint (h for hip, k for knee, and a for ankle) as well as the segment (D for distal and P for proximal) involved in the restriction. According to these equivalences, the unknown state vector of equation (2) for the

(a) Sensory systems used during experimental validation

(b) IMU's orientation in three different subjects

FIGURE 2. Sensor placement during the experimental essays. In panel (a), we highlighted the two sets of sensors involved in the experimental set-up. Orange inertial sensors are the Xsens sensors used as the gold standard for the calculus of the biomechanical model. In contrast, the sensors highlighted in blue are used to acquire the velocity and acceleration from gyroscopes and accelerometers to feed the Kalman algorithm. In panel (b), we show the placement of these sensors in three subjects that participated in the experimental validation. Ellipses of the same color mark the same sensor in each subject. The orientation of the same sensor slightly varied between subjects.

hip and ankle joints can be expressed as:

$$\bar{\mathbf{x}}_h = \begin{bmatrix} \alpha_{h_D} \\ \beta_{h_D} \\ \alpha_{h_P} \\ \beta_{h_P} \end{bmatrix} = \begin{bmatrix} \alpha_{k_P} \\ \beta_{k_P} \\ \alpha_{h_P} \\ \beta_{h_P} \end{bmatrix}; \quad \bar{\mathbf{x}}_a = \begin{bmatrix} \alpha_{a_D} \\ \beta_{a_D} \\ \alpha_{a_P} \\ \beta_{a_P} \end{bmatrix} = \begin{bmatrix} \alpha_{a_D} \\ \beta_{a_D} \\ \alpha_{k_D} \\ \beta_{k_D} \end{bmatrix} \tag{9}$$

Once the iterative problem was solved for the knee joint for the $i+1$ iteration, we use the estimation of the knee axis coordinates $\mathbf{v}_{k_D i+1}$ and $\mathbf{v}_{k_P i+1}$ to define the initial state vectors at the iteration i for the estimation of hip and ankle axes:

$$\bar{\mathbf{x}}_{h_i} = \begin{bmatrix} \alpha_{k_P i+1} \\ \beta_{k_P i+1} \\ \alpha_{h_P i} \\ \beta_{h_P i} \end{bmatrix}; \quad \bar{\mathbf{x}}_{a_i} = \begin{bmatrix} \alpha_{a_D i} \\ \beta_{a_D i} \\ \alpha_{k_D i+1} \\ \beta_{k_D i+1} \end{bmatrix} \tag{10}$$

Starting from these initial vectors, we can solve the equation (7) to estimate the state vectors $\bar{\mathbf{x}}_{h_{i+1}}$ and $\bar{\mathbf{x}}_{a_{i+1}}$ for the iteration $i+1$.

As explained in [2], signs of $\mathbf{v}_D$ and $\mathbf{v}_P$ need to match, i.e., the axis seen from both sensors, must point in the same direction. It can be achieved by maintaining a rough position that does not restrict the mounting orientation and defining the sign of one of the axis components; for example, the y-axis of the sensor must point laterally, and the y-component of the axis must remain positive.

C. EXPERIMENTAL VALIDATION

We tested the performance of this algorithm within eight healthy subjects (both sexes: 4 males, 4 females; age: 23.8±3.5 years; height: 1.7±0.07m; weight: 65.5±11.2kg; mean ± standard deviation). All subjects gave their informed consent for the experiment; the study was conducted in accordance with the Declaration of Helsinki, and it was approved by the local Ethics Committee (CSIC's Ethics Committee, approval number: 034/2020). Subjects were instructed to walk normally on a treadmill while sensor information was recorded. The inputs of our algorithm come from 4 (four) TechMCS IMUs (Technaid, Spain) that measured the raw angular velocity and acceleration. We strapped these sensors in arbitrary positions in the pelvis and the subjects' right thigh, shank, and foot (Fig. 2, panel a), being their orientation slightly different between subjects (Fig. 2, panel b). The initial orientation of these sensors was not modified during the execution of the trials.

We compared the estimation of our algorithm with the measurements obtained by an MVN system (Xsens Technologies B.V., Netherlands) as in other previous studies [46]–[48]. We used the quaternions provided by these sensors to run the OpenSense workflow of OpenSim open-source software [49], [50] and execute the biomechanical model defined in [51]. The results provided by OpenSense were used as the reference to assess the performance of our algorithm.

During the experimental trials, subjects walked on a treadmill at a constant velocity for 1 minute. Each subject repeated this trial three times at six different velocities (from 1km/h to 3km/h in 0.4km/h steps); the repetition order was set randomly. Data from the two sets of sensors were acquired at 50Hz.

III. RESULTS

Fig. 3 illustrates the comparison of the angles obtained by the Kalman filter with the result of the OpenSense biomechanical model for one of the trials. These results correspond to the movement of the hip, knee, and ankle joints in the sagittal plane: flexo/extension for hip and knee and dorsiflexion/plantarflexion for the ankle. Due to the uncertainty when the algorithm converges, there is an offset between the angles obtained by both methods. However, we can see the similarity

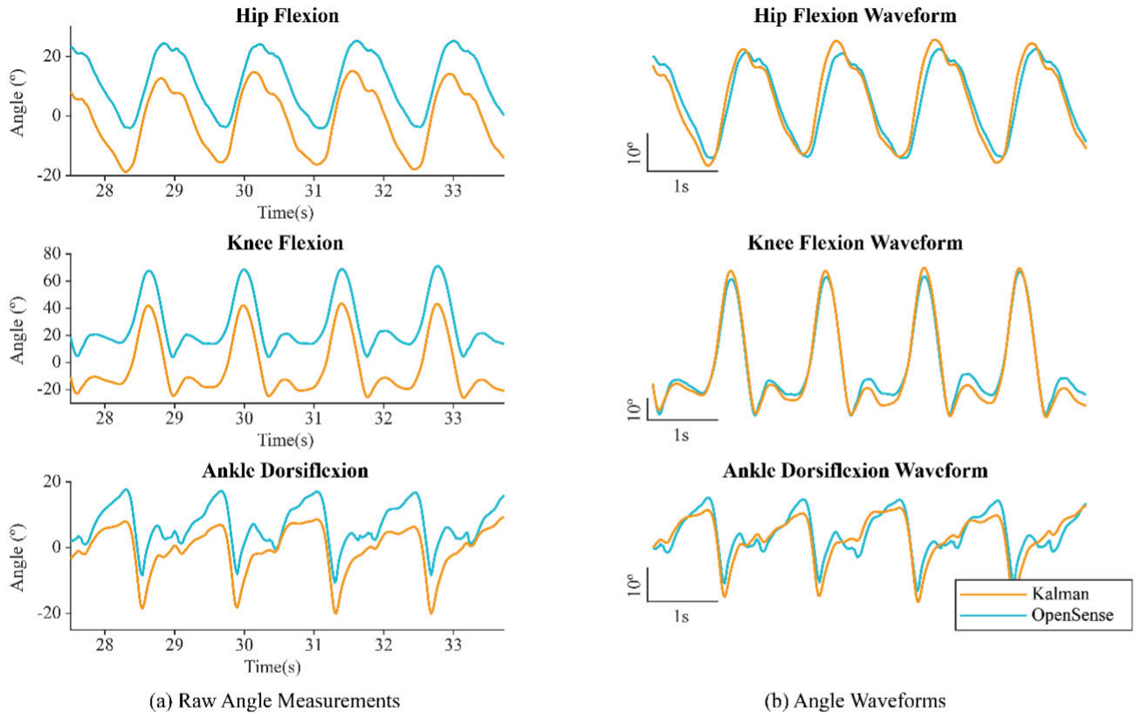

FIGURE 3. Angle estimation obtained by the Kalman algorithm (in orange) compared with the result obtained by OpenSense (in cyan). Panel (a) represents the raw results for hip flexion, knee flexion, and ankle dorsiflexion following both methods. Panel (b) represents the same results after removing the mean value and eliminating the offset.

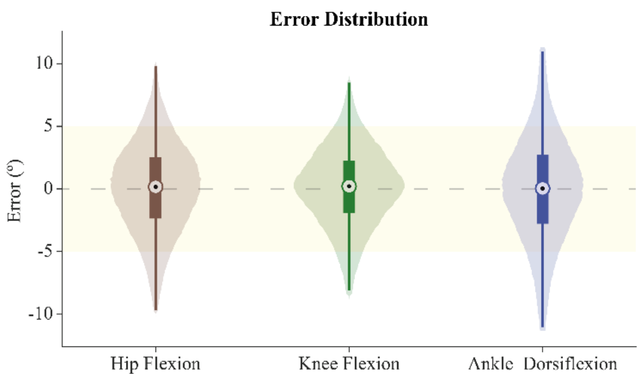

FIGURE 4. Violin plots for error distribution when comparing OpenSense and Kalman filter results. The shadowed areas represent the histogram of the data distributions, while boxplots represent the median, quartiles, and interquartile ranges of the distributions. We discarded data outliers from representation, corresponding to 1.3%, 2.5%, and 3.1% of hip, knee, and ankle samples. The highlighted region corresponds to errors between ±5°.

between both waveforms once we remove the average value of both curves (Fig. 3, Panel b). We discarded ankle data in three patients because the foot gyroscope was placed too close to the ankle joint and velocity measurements were erroneous.

To evaluate the algorithm's performance, we consider the waveform of the angles from the OpenSense simulation and the Kalman filter algorithm. These waveforms were calculated by removing the mean value from the kinematic signal.

$$\hat{\theta} = \theta - \bar{\theta} \tag{11}$$

TABLE 1. Summarized error in angle estimation.

Joint	Average Error (º) [a]	RMSE(º)
Hip	2.607e-15 ± 3.822	3.822
Knee	1.103e-14±3.602	3.602
Ankle	-3.245e-15 ± 4.844	4.844

[a] Mean value ± standard deviation

We calculated the error between both angle estimations according to the following equation:

$$\varepsilon = X_{OpenSense} - X_{Kalman} \tag{12}$$

where X is the variable whose error we aim to assess. This error definition will be used across this document.

Fig. 4 represents the error distributions for angle estimation in hip, knee, and ankle after pooling together the data from all subjects and trials. Average errors are close to zero, and RMS errors (RMSE) are 3.8°, 3.6°, and 4.8° for hip, knee, and ankle joints, respectively (Table 1).

During normal walking, it is highly probable that sensors slightly vary their initial orientation. Fig. 5 shows an example of one experimental trial during which the thigh IMU slightly moved from its original orientation. As the algorithm continuously estimates the joint axis direction, the algorithm reacts and corrects this estimation after the sensor's motion (Fig. 5, panel a and b). As it can be seen (Fig. 5, panel c), the effect over the angle estimation is transient, and it lasted until the new joint axis direction was reached.

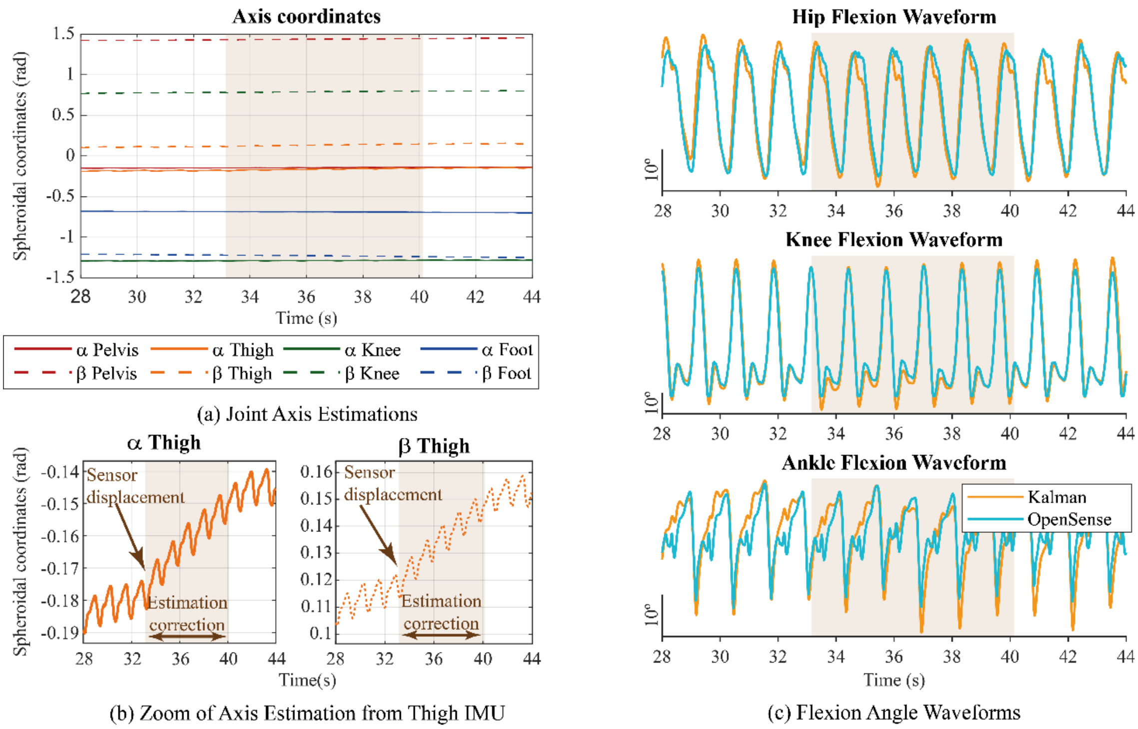

FIGURE 5. Example of the reaction of the algorithm to a slight sensor displacement during gait. Panel (a) shows the spheroidal coordinates of the estimation of the joint axes seen from the local coordinate system of each IMU (pelvis, thigh, knee, and foot). In Panel (b), we represent a zoom of the panel (a) to show the effect of a slight displacement in the thigh IMU; arrows point to the instant when the sensor changes its orientation, and the brown area represents the time while the algorithm corrected the estimation. In Panel (c), we represent the waveform estimation of hip, knee, and ankle flexion compared with the reference measure from OpenSense. Brown areas represent the same temporal window across panels. Notice how angle estimation is slightly affected due to sensor displacement, but this effect is corrected due to the new axis estimation.

TABLE 2. Key-Point definition for the assessment of the algorithm.

Joint	Id	Item	At	From	To
Hip	H1	Angle	Heel-Strike	-	-
	H2	Minimum angle	Stance	Heel-Strike	Toe Off
	H3	Angle	Toe-Off	-	-
	H4	Maximum angle	Swing	Toe-Off	Next Heel-Strike
Knee	K1	Angle	Heel-Strike	-	-
	K2	Maximum angle	Early Stance	Heel-Strike	Middle time between Heel-Strike and Toe-Off
	K3	Minimum angle	Terminal Stance	Middle time between Heel-Strike and Toe-Off	Toe-Off
	K4	Angle	Toe-Off	-	-
	K5	Maximum angle	Swing	Toe-Off	Next Heel-Strike
Ankle	A1	Angle	Heel-Strike	-	-
	A2	Minimum angle	Early Stance	Heel-Strike	Contralateral Toe-Off
	A3	Maximum angle	Terminal Stance	Heel-Strike	Toe-Off
	A4	Minimum angle	Swing	Toe-Off	Next Heel-Strike
	A5	Maximum angle	Terminal Swing	Toe-Off	Next Heel-Strike

A. KEY EVENTS DETECTION

To assess the capacity of our method to detect gait events for controlling wearable robots, we evaluated the detection of the key points for hip and knee flexo/extension and ankle dorsiflexion/plantarflexion defined in [52], [53] (Table 2). We adopted the method proposed by Bejarano *et al.* [54] to identify key events related to floor contact: Heel-Strike is defined as the minimum of the shank angle, and Toe-Off as the minimum of shank velocity. Fig. 6 illustrates the performance of the key-events detection in one trial.

During the experimental recordings, three subjects did not present a well-defined knee flexion movement during the stance phase. As a result, K2 (maximum early stance) and K3 (minimum terminal stance) key points were not calculated in these patients.

According to the error definition of the equation (12), we calculated the error in key-points detection concerning: i) time detection and ii) angular value of the joint waveform at this event. Fig. 7 and Table 3 summarize the error results in the detection of the key points. Average delays are close to zero,

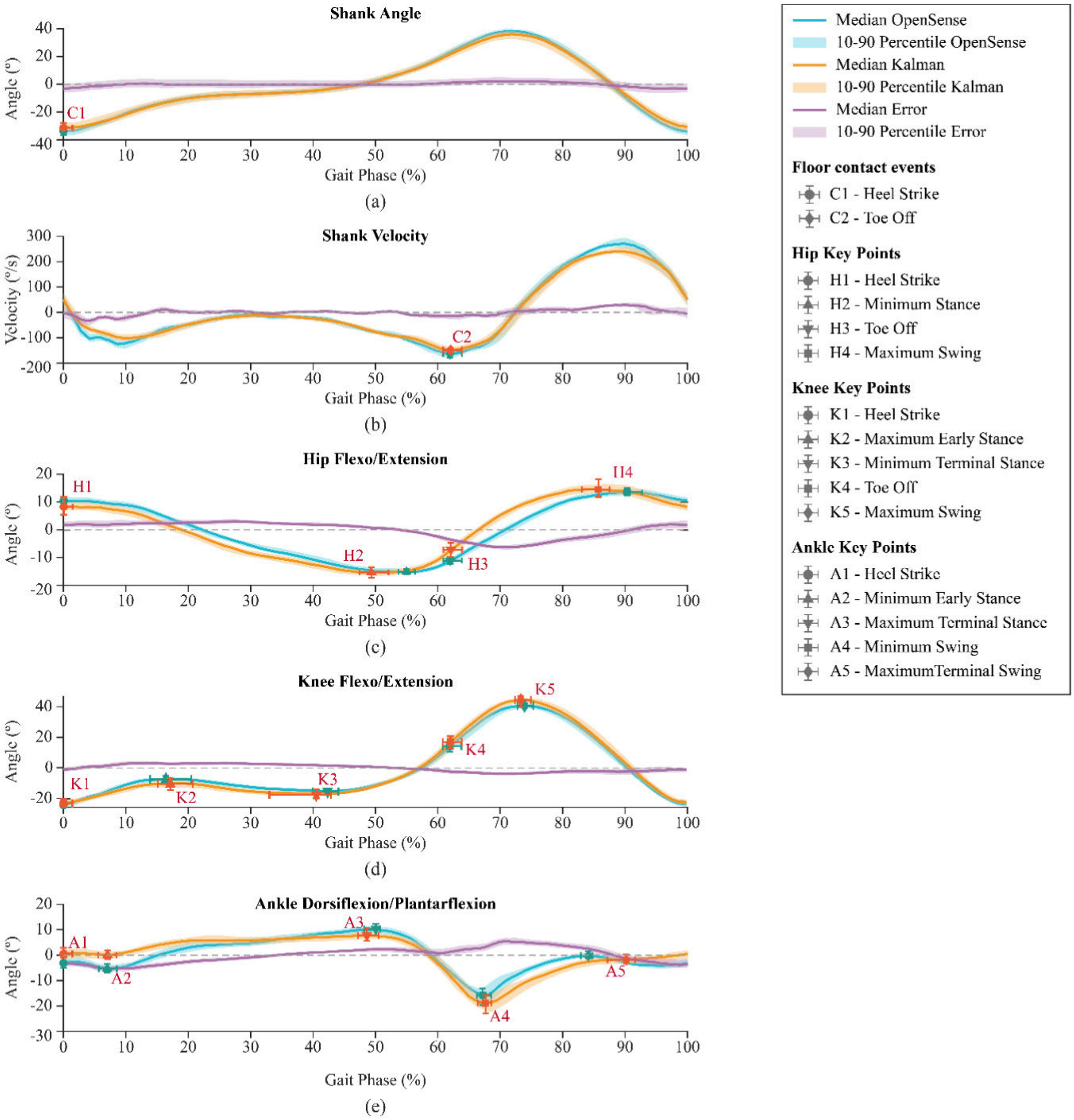

FIGURE 6. **Example of step kinematics and key-points detection during one trial. In all panels, we have compared the kinematics obtained with the OpenSense model (cyan) and the Kalman algorithm (orange), and we have also represented the error between both of them (purple). Step data are normalized to 0-100% of the gait cycle, considering the Heel-Strike detected based on OpenSense data as the beginning of the cycle. Solid lines represent the median value, while areas represent the 10-90 percentiles. Panels (a) and (b) represent the shank angle and velocity in the sagittal plane for the detection of the Heel-Strike and the Toe-Off, respectively. Panels (c), (d), and (e) represent the joint angle for the hip, knee, and ankle, respectively. In all panels, we have highlighted the corresponding Key-Points, accompanied by their labels. Markers represent the median location in the gait phase and angle; deviation whiskers indicate the 10-90 percentiles.**

and RMS delays are lower than 90ms for every key point. The average RMS delay for all Key-Points is 0.06s$\pm$0.02 (mean $\pm$ standard deviation). The average RMSE for all Key-Points is 4.2°$\pm$1.1 (mean $\pm$ standard deviation).

B. ADAPTIVE FREQUENCY OSCILLATOR

We also evaluated the quality of the information provided by our method to estimate in real-time the phase and frequency of the gait, data that could be used by a robotic exoskeleton controller. We used the AFO described in [55] with the heel-strike phase correction presented in [56].

We compared the results from this AFO with the real phase and frequency of the gait calculated offline. The inputs for the AFO were the joint angles and heel-strike computed with our extended Kalman filter, while the offline phase and frequency were computed with the heel-strike events detected based on

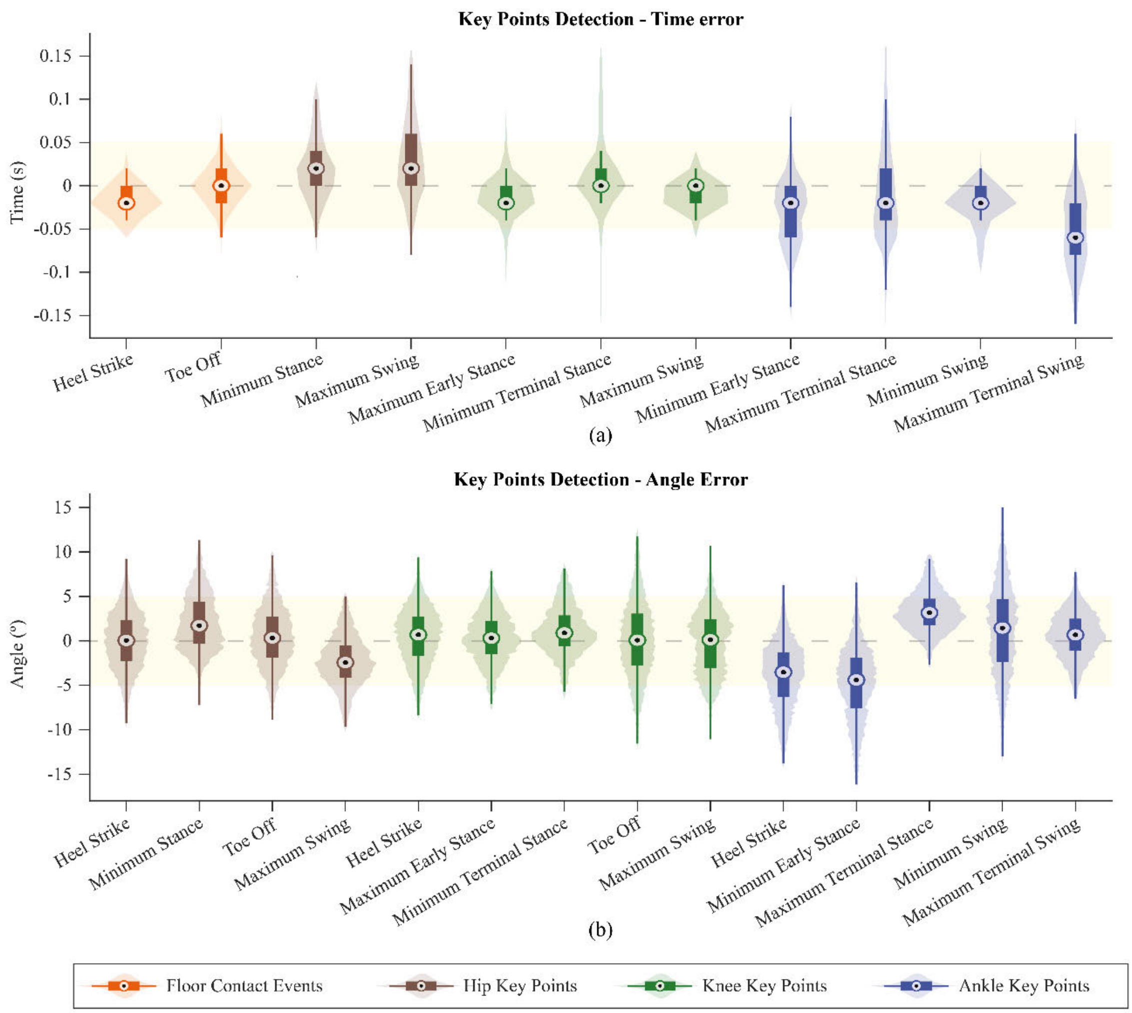

FIGURE 7. Violin plots for error distribution of key points detection when comparing OpenSense and Kalman algorithms. Panel (a) represents the error in time detection, and panel (b) represents the error in the angular value of the key point. Boxplots represent the median, quartiles, and interquartile ranges of the distributions, while shadowed areas represent the histogram of the data distributions. We have discarded outliers from representation; discarded data were lower than 10% of the total number of samples. The highlighted region corresponds to errors between ±0.05s and ±5° for time error and angle error, respectively.

the OpenSense model. Fig. 8 illustrates an example of the phase estimation during one trial for the kinematics of each joint.

Table 4 summarizes the error for the phase and frequency estimated with the AFO, and Fig. 9 shows the representation of the distributions, errors were calculated according to the error definition of the equation (12). Regarding the phase estimation, hip and knee RMSE are lower than 3.2%, although ankle RMSE is slightly higher than 8.5%. Hip and knee RMSE for frequency estimations are lower than 0.03Hz, although ankle RMSE is higher than 0.07Hz.

C. GAIT SPEED DEPENDENCY

Here we evaluate the dependency of the performance of the proposed algorithm with the gait speed. We looked for linear correlations between the measured errors (waveform errors, key-point detection errors, and frequency and phase estimation errors). However, none of these errors showed a significant relationship ($P < 0.01$) with the gait velocity of the subjects. Fig. 10. shows the correlation between waveform errors and gait velocities for the three joints, and Table 5 includes the results of the statistical analyses. Supplementary Figures 1-3 show regression models for key-points detection errors and frequency and phase estimation errors with respect to gait velocity. Supplementary Tables 1-2 contain the information about the statistical tests concerning the linear models.

IV. DISCUSSION

This paper introduces the formulation and experimental validation of an Extended Kalman Filter algorithm to estimate the sagittal movement of the hip, knee, and ankle joints during gait. This algorithm estimates the joint axes and the movement waveforms in real-time, based only on gyroscopes and accelerometers; consequently, it is unaffected by

TABLE 3. Average and RMS errors in the detection of key-points.

Key Point	Time Detection Error (s)		Angle Error (º)	
	Average Error [a]	RMSE	Average Error [a]	RMSE
C1: Heel Strike	-0.018±0.023	0.029	--	--
C2: Toe Off	0.003±0.030	0.030	--	--
H1: Heel Strike	--	--	-0.023±3.317	3.317
H2: Minimum Stance	0.022±0.048	0.053	2.116±3.190	3.827
H3: Toe Off	--	--	0.533±3.677	3.715
H4: Maximum Swing	0.041±0.060	0.073	-2.391±3.148	3.953
K1: Heel Strike	--	--	0.406±3.476	3.500
K2: Maximum Early Stance	-0.017±0.064	0.067	0.191±3.0972	3.103
K3: Minimum Terminal Stance	0.025±0.073	0.076	1.089±3.160	3.342
K4: Toe Off	--	--	0.469±5.030	5.051
K5: Maximum Swing	-0.008±0.018	0.020	-0.209±3.662	3.667
A1: Heel Strike	--	--	-3.905±3.811	5.456
A2: Minimum Early Stance	-0.042±0.076	0.087	-4.704±4.588	6.571
A3: Maximum Terminal Stance	0.004±0.087	0.087	3.475±2.728	4.417
A4: Minimum Swing	-0.031±0.039	0.050	1.039±5.337	5.437
A5: Maximum Terminal Swing	-0.056±0.048	0.074	0.633±2.821	2.891
Average RMSE [a]	0.059±0.024		4.161±1.079	

[a] Mean value ± standard deviation

TABLE 4. Summarized errors in gait phase and frequency estimation.

Joint	Phase (gait cycle %)		Frequency (Hz)	
	Average Error [a]	RMSE	Average Error [a]	RMSE
Hip	1.014±2.701	2.885	6.7Ee-5±0.021	0.021
Knee	1.228±2.863	3.115	1.4e-4±0.024	0.024
Ankle	4.469±7.489	8.721	0.032±0.072	0.079

[a] Mean value ± standard deviation

magnetic disturbances. As this algorithm is able to continuously estimate the joint axes in the local coordinate system of the sensors, it is not necessary to align the sensor axes with the segments of the body. Notably, the algorithm does not require any previous calibration for the estimation of the joint axes; it estimates them during the user's first steps and continuously updates these estimations in real-time. Although we have run the algorithm offline, it can be directly used in real-time without any change. Actually, in our previous work [45], we reported the real-time implementation on a microcontroller of an earlier version of this algorithm that only involved the knee joint. More powerful hardware like a dual-core microcontroller or a single-board computer must deal with the computational cost of running the current algorithm in real-time.

In general, the quality of the ankle estimation is lower than for the hip and knee joints. Mainly, it is because the angular velocity in the ankle joint is lower than in the other two joints during most of the gait cycle; thus, the signal-noise ratio is worse than for the hip and the knee. According to [48], a good estimation requires that the motion is rich enough to fulfill the constraints; in this sense, the algorithm is able to yield better results in hip and knee joints as their angular velocities are higher during most of the gait cycle.

On the other hand, ankle and hip errors are higher than knee errors because we used a hinge joint to model these three joints. This model is more accurate for the knee than for the other joints, which can move in the three anatomic planes and not only in the sagittal one; however, the low attained RMSE for the ankle and hip joints enable this algorithm to be used in the three joints.

Compared with previously published works, our method yields slightly higher errors than other methods that also use gyroscopes and accelerometers [3]; nevertheless, it does not require any previous alignment or calibration, allowing for a quicker set-up. We yielded similar RMSE than Seel *et al.* for the knee joint (their result was 3.3° while ours is 3.6°) and worse RMSE for the ankle joint (4.8° against 1.6°) [2]. Compared with our method, they also estimated the joint axes, although they did it offline and based on calibration motion. Joukov *et al.* also obtained better RMSE than us (lower than 2.4°) in the lower limb kinematic estimation [7]. They used a method based on a Rhythmic Extended Kalman Filter; however, they also needed to calibrate the model and align the local IMUs frames with joints frames. Other methods that also yielded lower RMSE errors relied on anthropometric measurements of the subjects [5], [10] or needed to train subject-specific models [57], [58].

Compared with these approaches, although our method is not as accurate, it is easier to don, and it does not need previous calibration movements, so it increases its value as a sensor system for controlling wearable devices. Our approach is also more robust than the other alternatives to sensor displacements during measurements. Since we continuously calculate the joint axis direction, our method reacts to sensors displacement by correcting the axis estimation in real-time. All these features enable the possibility of using this approach to assist daily life activities in a domestic non-supervised environment.

The proposed method was designed to allow inertial sensors to be used as input information for controllers of lower-limb wearable robotic devices, for example, by detecting gait events that could act as states in a finite-state machine or

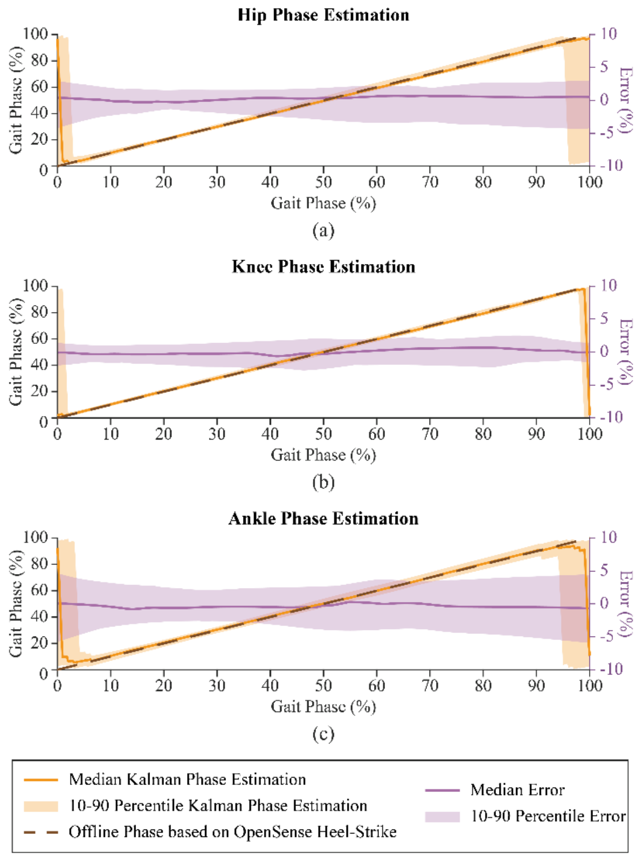

FIGURE 8. Example of phase estimation during one trial when hip (Panel a), knee (Panel b), or ankle (Panel c) kinematics are used as input of an AFO. The phase estimated was represented (orange line) and compared with the real gait phase (dashed brown line). The error between them is also depicted with respect to the right axis (purple line). Shadowed areas represent the 10-90 percentiles of the signals.

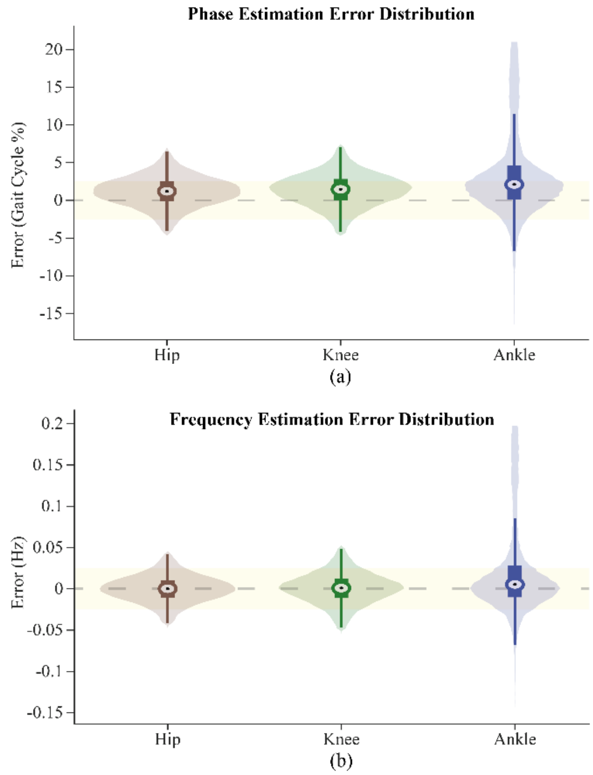

FIGURE 9. Error distributions for the phase (Panel a) and frequency (Panel b) estimated with the AFO based on the kinematics resulted from the Kalman filter. The shadowed areas represent the histogram of the data distributions, while boxplots represent the median, quartiles, and interquartile ranges. Outlier data were discarded from the representation, being less than 5% of the total of samples. The highlighted region corresponds to errors between ±2.5% and ±0.025Hz for phase and frequency estimation, respectively.

estimating the gait phase in real-time. We assessed the performance of this method for the detection of gait key events related to the waveform of the joint's motion. The yielded average RMS delay is about 60ms, which corresponds to only three sensor data samples.

Compared with other published methods, ours performed similarly when detecting contact events. Our experimental validation arose average errors for detecting heel-strike and toe-off of −18±23ms and 3±30ms, respectively. Maqbool *et al.* used similar data, as they used an IMU placed at the shank of the users [59]. By using a real-time heuristic approach, they reported average errors of 16±9ms and −13±15.9ms for initial contact and toe-off, respectively. Similarly, Sahoo *et al.* also used a rule-based method with shank-placed IMUs data and reported average errors of 10.4±26.5ms and −13.7±76.6ms for these same events [42]. However, other studies reported better results than ours, although they used different approaches. For example, Boutaayamou *et al.* yielded average errors of 1.3±7.2ms and −1.8±11.8ms for detecting heel-strike and toe-off by using accelerometers attached to the heel and the toe [60]. Similarly, Mariani *et al.* reported average errors of 1±13ms and −3±13ms for both events using foot-worn inertial sensors [61].

In spite of our slightly poorer results, according to the analysis in [42], small differences in the order of milliseconds would not affect practical scenarios. In addition, unlike these previous works, which were focused only on contact events, our approach also provides information about other relevant events related to the maximum and minimum of the flexion/extension movements of the joints.

According to [62], [63], delays lower than 150ms are valid for online functional electrical stimulation, and Figueiredo *et al.* [64] consider that delays of few tenths of milliseconds are acceptable for the control of robotic exoskeletons as they are lower than the reaction time of voluntary muscle contractions (180ms). Therefore, we can conclude that the presented algorithm can be considered valid to detect gait events to control wearable robotic devices. Noticeably, a previous approach of this method was validated to control a quasi-passive exosuit for space activities by detecting knee kinematics key events [65].

We have also assessed the performance of an AFO when we use the estimated waveforms as inputs. Results pointed out that AFO performance worsens when using ankle data,

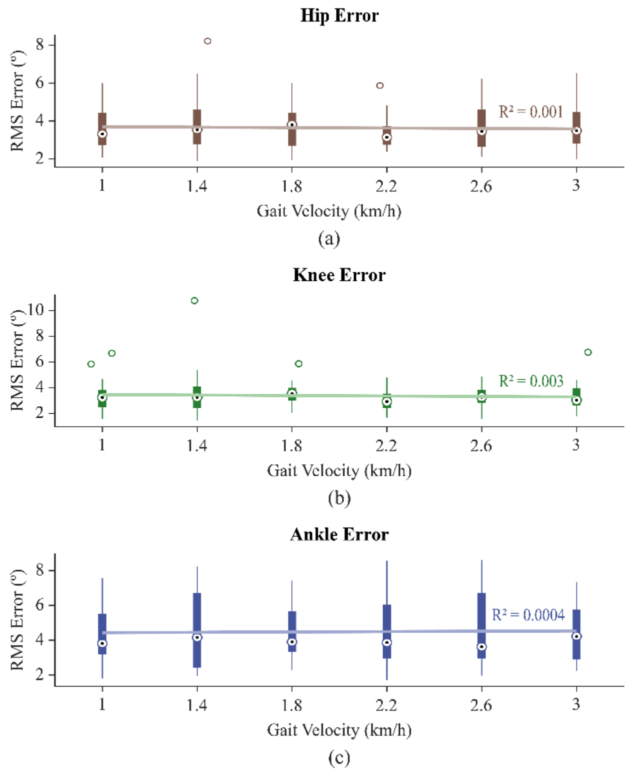

FIGURE 10. Linear regression between gait velocity and waveform errors for the three joints. Panels (a) – (c) represent the relationships between gait velocity and trial RMS errors for the hip, knee, and ankle joints, respectively. Boxplots represent the error distribution at each velocity; the straight lines represent the regression calculated for each joint.

TABLE 5. Statistical results for the regression models between gait velocity and waveform error estimation.

Joint	P-value	R^2
Hip	0.687	0.001
Knee	0.567	0.003
Ankle	0.846	0.0004

as RMSE is about three times more than when AFO uses hip or knee information. According to Ruiz-Garate *et al.*, we can consider that phase estimation is synchronized with gait if the error is lower than 10% [66]. In this regard, phase estimations are valid for controlling a robotic device as the phase estimation RMSEs are lower than this threshold in the three joints.

Compared with the results obtained by AFOs in other studies, the estimation based on ankle data is not as accurate. However, the estimations based on the knee and hip kinematics (with RMSE about 3.1% and 2.8%, respectively) are similar or slightly poorer. Other authors reported a phase estimation RMSE of 3% using noncontact capacitive sensors [67], 2% using insole pressure sensors to measure the vertical ground reaction force [68], or 1.4% using an encoder to measure the hip angle [68]. However, the apparatus required for our algorithm is more robust than pressure-based sensors and easier to don than capacitive sensors or exoskeleton-embedded sensors.

Finally, we did not find relations between gait velocity and the performance of the algorithm. We analyzed the gait velocity range between 1km/h and 3km/h, and no correlations were found between gait speed and RMSE in the kinematics or the results of key-events detection or AFO estimations. Although varying gait speeds were not directly assessed, this method would not be affected by them. Our approach already considers changing instantaneous velocity measurements due to the normal gait cycle, and, on the other hand, a changing gait speed would not affect the biomechanical basis of our approach, as suggested by the results of our previously published work [45]

Apart from the experimental conditions reported in this paper, our method should be valid as long as the movement around the sagittal axis is rich enough to fulfill the one-axis restriction in the knee joint [48]. This suggests that this algorithm could also be applied in other contexts as outdoor environments or with impaired subjects. Hawkins *et al.* reported that healthy subjects walking on uneven terrain usually adapt their gait to increase balance and stability by slowing down their gait velocity or increasing hip and knee flexion and ankle dorsiflexion movements [69]. These adaptations would not interfere with the performance of the proposed algorithm, as it does not modify its biomechanical basis, and we have assessed its correct performance even at low gait speed (1km/h). This low gait speed is also characteristic of impaired subjects [70], who also could use this approach as long as they were able to generate movement in their lower limb joints. However, it would still be necessary to validate the performance of this algorithm experimentally under these circumstances.

V. CONCLUSION

This paper presents a new algorithm based on an Extended Kalman Filter for real-time estimation of lower limb kinematics that can be used as a basis for lower-limb wearable robot controllers. As the algorithm does not use magnetometer data, it is not affected by electromagnetic disturbances in the environment. In addition, as the proposed algorithm continuously estimates the sagittal joint axis, it does not need any prior calibration or alignment, which eases donning the system and enables it to be used in daily life. After assessing the algorithm, RMSE errors about 3.8°, 3.6°, and 4.8° for hip, knee, and ankle flexion in the sagittal plane, and gait event detection delays and phase estimation errors under the required threshold confirm that the proposed method is a feasible solution to control lower-limb wearable robotic devices.

APPENDIX

To solve the posed problem, we used the following nonlinear state-space discrete form representation of the process and measurement models

$$\mathbf{x}_{j+1} = \mathbf{f}(\mathbf{x}_j, \mathbf{u}_j, j) + \mathbf{m}_j; \quad \mathbf{z}_j = \mathbf{h}(\mathbf{x}_j, j) + \mathbf{n}_j \tag{13}$$

where $\mathbf{x}$, $\mathbf{u}$ and $\mathbf{z}$ are the state, control and measurement vectors at instant j and $\mathbf{m} \sim \mathcal{N}(0, \mathbf{Q})$ and $\mathbf{n} \sim \mathcal{N}(0, \mathbf{R})$ represent uncorrelated Gaussian processes with zero mean and covariance matrices $\mathbf{Q}$ and $\mathbf{R}$. Considering the nominal state vector $\hat{\mathbf{x}}$ as the state vector without the process noise, the error $\tilde{\mathbf{x}}$ due to this noise, at time *j+1* can be expressed as

$$\tilde{\mathbf{x}}_{j+1} = \mathbf{f}(\mathbf{x}_j, \mathbf{u}_j, j) + \mathbf{m}_j - \hat{\mathbf{x}}_{j+1} \tag{14}$$

As function $\mathbf{f}(\mathbf{x}_j, \mathbf{u}_j, j)$ can be approximated by means of a Taylor expansion around the state vector $\hat{\mathbf{x}}_j$, the error $\tilde{\mathbf{x}}_{j+1}$ can be defined as follow,

$$\begin{aligned}\tilde{\mathbf{x}}_{j+1} &= \left.\frac{\partial \mathbf{f}(\mathbf{x}, \mathbf{u}, j)}{\partial \mathbf{x}}\right|_{\mathbf{x}=\hat{\mathbf{x}}_j} \tilde{\mathbf{x}}_j + \mathbf{m}_j \\ &= \mathbf{\Phi}(\hat{\mathbf{x}}_j, \mathbf{u}_j, j)\tilde{\mathbf{x}}_j + \mathbf{m}_j \end{aligned} \tag{15}$$

with $\mathbf{\Phi}(\hat{\mathbf{x}}_j, j)$ as a state transition matrix. Therefore, (14) can be linearized by taking the dynamics of the error $\tilde{\mathbf{x}}$ into account.

Using an analogue procedure, the error in the measurement vector $\tilde{\mathbf{z}}_j$ is linearized around the state vector $\hat{\mathbf{x}}_j$ as follow,

$$\tilde{\mathbf{z}}_j = \mathbf{H}(\hat{\mathbf{x}}_j, j)\tilde{\mathbf{x}}_j + \mathbf{n}_j \tag{16}$$

where the matrix $\mathbf{H}(\hat{\mathbf{x}}_j, j)$ is the Jacobian of the measurement matrix $\mathbf{h}(\mathbf{x}_j, j)$.

A. PROCESS MODEL EQUATIONS

As we are interested on estimating the joint rotation angle around the sagittal axis, the state vector of the process model must be determined. The joint angular velocity $\dot{\theta}_j$ at each time instant j can be calculated as follow

$$\dot{\theta}_j = (\boldsymbol{\omega}_{1j}^T\, \mathbf{v}_1 + bias_1) - (\boldsymbol{\omega}_{2j}^T\, \mathbf{v}_2 + bias_2) + \eta_{\dot{\theta}} \tag{17}$$

where $\boldsymbol{\omega}_{1j}$ and $\boldsymbol{\omega}_{2j}$ are the angular velocities measured by the inertial sensors attached to the segments of the limb at the time j, $\mathbf{v}_1$ and $\mathbf{v}_2$ are the local coordinates of the sagittal joint axis and $bias_1$, $bias_2$ and $\eta_{\dot{\theta}}$ are the biases and noise of the measurements

To compute the joint rotation angle, an offset term has also been considered, which leads to

$$\begin{aligned}\theta_j &= h_\theta(\mathbf{v}_1, \mathbf{v}_2, bias_1, bias_2, offset) + \eta_\theta \\ \theta_j &= \theta_{j-1} + \dot{\theta}_j \Delta h + offset + \eta_\theta \end{aligned} \tag{18}$$

where Δh is the sample time of the measurements.

Additional constraints can be defined by considering the transformation matrix $\mathbf{R}_{12}$ that links the estimation of the local coordinates of the sagittal joint rotation axis $\mathbf{v}_1$ and $\mathbf{v}_2$. This same matrix is used to transform the coordinates of unitary vectors in the direction of gravity $\mathbf{g}_1$ and $\mathbf{g}_2$ from both coordinate system, giving us the constrain $\mathbf{e}_g$.

$$\mathbf{g}_1 = \mathbf{R}_{12}\mathbf{g}_2 \Rightarrow \mathbf{e}_g = \mathbf{g}_1 - \mathbf{R}_{12}\mathbf{g}_2 \tag{19}$$

Assuming that the gravity and rotation vectors are not coincident and that the joint rotation movement can be modelled as a rigid transformation, the cross products $\mathbf{L}_1 = \mathbf{g}_1 \times \mathbf{v}_1$ and $\mathbf{L}_2 = \mathbf{g}_2 \times \mathbf{v}_2$ are preserved. In this way, the vectors $\mathbf{L}_1$ and $\mathbf{L}_2$ are related by the next equation, giving us an additional kinematic constrain $\mathbf{e}_L$.

$$\mathbf{L}_1 = \mathbf{R}_{12} \times \mathbf{L}_2 \Rightarrow \mathbf{e}_L = \mathbf{L}_1 - \mathbf{R}_{12} \times \mathbf{L}_2 \tag{20}$$

Using the constraint defined in (4), and due to the fact that $\mathbf{R}_{12}$ links the coordinate of $\mathbf{v}_1$ and $\mathbf{v}_2$, this constraint can be redefined as

$$\mathbf{e}(\mathbf{R}_{12}, \mathbf{v}_2)_j = ||\boldsymbol{\omega}_{1j} \times \mathbf{R}_{12}\mathbf{v}_2|| - ||\boldsymbol{\omega}_{2j} \times \mathbf{v}_2|| \tag{21}$$

Therefore, we can define a constrain vector with (19), (20) and (21):

$$\mathbf{e}(\mathbf{R}_{12}, \mathbf{v}_2, \mathbf{g}_2, \mathbf{L}_2) = [\mathbf{e}_1\ \mathbf{e}_2 \ldots \mathbf{e}_N\ \mathbf{e}_g \mathbf{e}_L]^T \tag{22}$$

Considering the exponential map of rotation matrices, the transformation matrix $\mathbf{R}_{12}$ can be written as

$$\mathbf{R}_{12}(\mathbf{b}, \gamma) = e^{\hat{\mathbf{b}}\gamma} = \mathbf{I} + \hat{\mathbf{b}}\, sin\gamma + \hat{\mathbf{b}}^2\, (1 - cos\gamma) \tag{23}$$

where $\mathbf{b}$ is the unitary rotation vector, γ is the rotation angle and $\hat{\mathbf{b}}$ is the skew-symmetric matrix such $\hat{\mathbf{b}} \in so(3)$. By considering that the spheroidal coordinates of the rotation axes $\mathbf{v}_1$ and $\mathbf{v}_2$, the components of vectors $\bar{\mathbf{x}}_j$ and $\tilde{\bar{\mathbf{x}}}_j$ at a time j will be

$$\bar{\mathbf{x}}_j = [\alpha_1\ \beta_1\ \alpha_2\ \beta_2\ \gamma]^T; \quad \tilde{\bar{\mathbf{x}}}_j = [\tilde{\alpha}_1\ \tilde{\beta}_1\ \tilde{\alpha}_2\ \tilde{\beta}_2 \tilde{\gamma}]^T \tag{24}$$

where the tilde variables indicate the estimation error.

Then, as an error vector $\tilde{\bar{\mathbf{x}}}$ can be included into the state vector (shown by the linearization of (15)), the state vector $\tilde{\mathbf{x}}$ is defined as follow

$$\begin{aligned}\tilde{\mathbf{x}} &= [\mathbf{x}\ \tilde{\bar{\mathbf{x}}}]^T; \mathbf{x}_\theta = [\theta\ \dot{\theta}]^T \\ \tilde{\bar{\mathbf{x}}} &= [\tilde{\alpha}_1\ \tilde{\beta}_1\ \tilde{\alpha}_2\ \tilde{\beta}_2\ \tilde{\gamma} \widetilde{bias_1}\ \widetilde{bias_2}\ \widetilde{offset}]^T \end{aligned} \tag{25}$$

Assuming that the constraints error vector $\tilde{\bar{\mathbf{x}}}$ is linear, the state transition matrix will be defined as

$$\mathbf{\Phi} = \begin{bmatrix} \partial \mathbf{h}(\mathbf{v}_1, \mathbf{v}_2, bias_1, bias_2, offset) / \partial \tilde{\mathbf{x}} \\ \mathbf{\Phi}_e \end{bmatrix} = \begin{bmatrix} \mathbf{h}_{\tilde{\mathbf{x}}} \\ \mathbf{\Phi}_e \end{bmatrix} \tag{26}$$

with $\mathbf{h}$ and Φ_e being

$$\begin{aligned}\mathbf{h}(\mathbf{v}_1, \mathbf{v}_2, bias_1, bias_2, offset) &= \begin{bmatrix} h_\theta & h_{\dot{\theta}} \end{bmatrix}^T \\ \mathbf{\Phi}_e &= \begin{bmatrix} \mathbf{0}_{8\times 2} & \mathbf{I}_{8\times 8} \end{bmatrix}_{8\times 10} \end{aligned} \tag{27}$$

with $\mathbf{I}$ being the 8×8 identity matrix.

So, the equation of the process model (15) is redefined as

$$\begin{bmatrix} \mathbf{x}_\theta \\ \tilde{\bar{\mathbf{x}}} \end{bmatrix}_{j+1} = \begin{bmatrix} \mathbf{h}_{\tilde{\mathbf{x}}} \\ \mathbf{\Phi}_e \end{bmatrix} \begin{bmatrix} \mathbf{x}_\theta \\ \tilde{\bar{\mathbf{x}}} \end{bmatrix}_j + \mathbf{m}_j \tag{28}$$

The covariance matrix $\mathbf{Q}$ has been computed using the standard deviation of the IMUs and following the equations of the process model in the error of the state vector. The standard deviation of the bias and offset variables have been considered equal to zero.

B. MEASUREMENT MODEL EQUATIONS

To estimate a state vector $\bar{\mathbf{x}}$, we can rely on a set of constraints that try to minimize errors $\mathbf{e}(\bar{\mathbf{x}}, j) = \mathbf{0}$ which are functions of the state vector $\bar{\mathbf{x}}$ to be estimated. If we suppose that a linear approximation of the constrain functions $\mathbf{e}(\bar{\mathbf{x}}, j)$ around an initial guess of the solution $\bar{\mathbf{x}}$ designated as $\bar{\bar{\mathbf{x}}}$ is done by means of a Taylor series expansion. The error $\tilde{\bar{\mathbf{x}}} = (\bar{\mathbf{x}} - \bar{\bar{\mathbf{x}}})$ can be computed by the following linear equality

$$\mathbf{e}(\bar{\mathbf{x}}, j) = \mathbf{e}(\bar{\bar{\mathbf{x}}}, j) + \left.\frac{\partial \mathbf{e}(\bar{\mathbf{x}}, j)}{\partial \bar{\mathbf{x}}}\right|_{\bar{\mathbf{x}}=\bar{\bar{\mathbf{x}}}} (\bar{\mathbf{x}} - \bar{\bar{\mathbf{x}}}) \tag{29}$$

In this way, considering that we are measuring the error $\mathbf{e}(\bar{\mathbf{x}}, j) = \mathbf{0}$, the equation (29) can be used to write the measurement model in the following way

$$-\mathbf{e}(\bar{\bar{\mathbf{x}}}_j, j) = \mathbf{G}(\bar{\bar{\mathbf{x}}}_j, j)\tilde{\bar{\mathbf{x}}}_j + \mathbf{n}_j = \tilde{\bar{\mathbf{z}}}_j \tag{30}$$

where the matrix $\mathbf{G}(\bar{\bar{\mathbf{x}}}_j, j)$ is the Jacobian of the error vector.

The measurement model of (30) indicates that the error constitutes the state vector, while the vector $\mathbf{n}_j$ represents the noise term. As there are not sensors to measure $\bar{\mathbf{z}}_j$, these virtual measurements will be supposed to be equal to zero $\bar{\mathbf{z}}_j = \mathbf{0}$, this assumption requiring the measurement errors to be considered into the measurement covariance matrix $\mathbf{R}$.

In this way, considering the state vector of the process model of (28) and the virtual measurement of (30), the measurement model equation is defined by

$$\begin{bmatrix} \mathbf{0} \\ \tilde{\bar{\mathbf{z}}}_j \end{bmatrix} = \begin{bmatrix} \mathbf{I}_{2\times 2} & \mathbf{0} \\ \mathbf{0} & \mathbf{G}(\bar{\bar{\mathbf{x}}}_j, j) \end{bmatrix} \begin{bmatrix} \mathbf{x}_\theta \\ \tilde{\bar{\mathbf{x}}} \end{bmatrix}_j + \mathbf{n}_j \tag{31}$$

The covariance matrix $\mathbf{R}$ has been computed considering that the variables of the measurement matrix are proportional to the variances of the IMUs in accordance with the IMU local frames where they are being computed.

REFERENCES

[1] I. H. Lopez-Nava and M. M. Angelica, "Wearable inertial sensors for human motion analysis: A review," *IEEE Sensors J.*, vol. 16, no. 22, pp. 7821–7834, Nov. 2016.
[2] T. Seel, J. Raisch, and T. Schauer, "IMU-based joint angle measurement for gait analysis," *Sensors*, vol. 14, no. 4, pp. 6891–6909, Jan. 2014.
[3] I. Weygers, M. Kok, M. Konings, H. Hallez, H. De Vroey, and K. Claeys, "Inertial sensor-based lower limb joint kinematics: A methodological systematic review," *Sensors*, vol. 20, no. 3, pp. 1–23, 2020.
[4] A. M. Sabatini, "Quaternion-based strap-down integration method for applications of inertial sensing to gait analysis," *Med. Biol. Eng. Comput.*, vol. 43, no. 1, pp. 94–101, Feb. 2005.
[5] S. Tadano, R. Takeda, and H. Miyagawa, "Three dimensional gait analysis using wearable acceleration and gyro sensors based on quaternion calculations," *Sensors*, vol. 13, no. 7, pp. 9321–9343, Jul. 2013.
[6] K. J. O'Donovan, R. Kamnik, D. T. O'Keeffe, and G. M. Lyons, "An inertial and magnetic sensor based technique for joint angle measurement," *J. Biomech.*, vol. 40, no. 12, pp. 2604–2611, 2007.
[7] V. Joukov, V. Bonnet, M. Karg, G. Venture, and D. Kulic, "Rhythmic extended Kalman filter for gait rehabilitation motion estimation and segmentation," *IEEE Trans. Neural Syst. Rehabil. Eng.*, vol. 26, no. 2, pp. 407–418, Feb. 2018.
[8] S. Šlajpah, R. Kamnik, and M. Munih, "Kinematics based sensory fusion for wearable motion assessment in human walking," *Comput. Methods Programs Biomed.*, vol. 116, no. 2, pp. 131–144, 2014.
[9] E. Dorschky, M. Nitschke, A.-K. Seifer, A. J. van den Bogert, and B. M. Eskofier, "Estimation of gait kinematics and kinetics from inertial sensor data using optimal control of musculoskeletal models," *J. Biomech.*, vol. 95, Oct. 2019, Art. no. 109278.
[10] V. Bonnet, V. Joukov, D. Kulić, P. Fraisse, N. Ramdani, and G. Venture, "Monitoring of hip and knee joint angles using a single inertial measurement unit during lower limb rehabilitation," *IEEE Sensors J.*, vol. 16, no. 6, pp. 1557–1564, Mar. 2016.
[11] B. Fasel, J. Spörri, J. Chardonnens, J. Kröll, E. Müller, and K. Aminian, "Joint inertial sensor orientation drift reduction for highly dynamic movements," *IEEE J. Biomed. Health Inform.*, vol. 22, no. 1, pp. 77–86, Jan. 2018.
[12] S. Choi, Y. B. Shin, S.-Y. Kim, and J. Kim, "A novel sensor-based assessment of lower limb spasticity in children with cerebral palsy," *J. NeuroEng. Rehabil.*, vol. 15, no. 1, pp. 1–16, Dec. 2018.
[13] J. Cockcroft, J. H. Muller, and C. Scheffer, "A novel complimentary filter for tracking hip angles during cycling using wireless inertial sensors and dynamic acceleration estimation," *IEEE Sensors J.*, vol. 14, no. 8, pp. 2864–2871, Aug. 2014.
[14] E. R. Bachmann, X. Yun, and A. Brumfield, "Limitations of attitude estimation algorithms for inertial/magnetic sensor modules," *IEEE Robot. Autom. Mag.*, vol. 14, no. 3, pp. 76–87, Sep. 2007.
[15] W. H. K. de Vries, H. E. J. Veeger, C. T. M. Baten, and F. C. T. van der Helm, "Magnetic distortion in motion labs, implications for validating inertial magnetic sensors," *Gait Posture*, vol. 29, no. 4, pp. 535–541, 2009.
[16] J. Favre, R. Aissaoui, B. M. Jolles, J. A. de Guise, and K. Aminian, "Functional calibration procedure for 3D knee joint angle description using inertial sensors," *J. Biomech.*, vol. 42, no. 14, pp. 2330–2335, 2009.
[17] A. Rodríguez-Fernández, J. Lobo-Prat, and J. M. Font-Llagunes, "Systematic review on wearable lower-limb exoskeletons for gait training in neuromuscular impairments," *J. NeuroEng. Rehabil.*, vol. 18, no. 1, pp. 1–21, Dec. 2021.
[18] B. Hobbs and P. Artemiadis, "A review of robot-assisted lower-limb stroke therapy: Unexplored paths and future directions in gait rehabilitation," *Frontiers Neurorobot.*, vol. 14, p. 19, Apr. 2020.
[19] B. Kalita, J. Narayan, and S. K. Dwivedy, "Development of active lower limb robotic-based orthosis and exoskeleton devices: A systematic review," *Int. J. Social Robot.*, vol. 13, no. 4, pp. 775–793, Jul. 2021.
[20] R. Baud, A. R. Manzoori, A. Ijspeert, and M. Bouri, "Review of control strategies for lower-limb exoskeletons to assist gait," *J. NeuroEng. Rehabil.*, vol. 18, no. 1, pp. 1–34, Dec. 2021.
[21] D. Shi, W. Zhang, W. Zhang, and X. Ding, "A review on lower limb rehabilitation exoskeleton robots," *Chin. J. Mech. Eng.*, vol. 32, no. 1, pp. 1–11, Dec. 2019.
[22] M. S. Al-Quraishi, I. Elamvazuthi, S. A. Daud, S. Parasuraman, and A. Borboni, "EEG-based control for upper and lower limb exoskeletons and prostheses: A systematic review," *Sensors*, vol. 18, no. 10, pp. 1–27, 2018.
[23] G. Yin, X. Zhang, D. Chen, H. Li, J. Chen, C. Chen, and S. Lemos, "Processing surface EMG signals for exoskeleton motion control," *Frontiers Neurorobot.*, vol. 14, p. 40, Jul. 2020.
[24] A. Wall, J. Borg, and S. Palmcrantz, "Clinical application of the hybrid assistive limb (HAL) for gait training—A systematic review," *Frontiers Syst. Neurosci.*, vol. 9, p. 48, Mar. 2015.
[25] Y. Mengüç, Y. L. Park, H. Pei, D. Vogt, P. M. Aubin, E. Winchell, L. Fluke, L. Stirling, R. J. Wood, and C. J. Walsh, "Wearable soft sensing suit for human gait measurement," *Int. J. Robot. Res.*, vol. 33, no. 14, pp. 1748–1764, 2014.
[26] M. Totaro, T. Poliero, A. Mondini, C. Lucarotti, G. Cairoli, J. Ortiz, and L. Beccai, "Soft smart garments for lower limb joint position analysis," *Sensors*, vol. 17, no. 10, p. 2314, Oct. 2017.
[27] H. Souri, H. Banerjee, A. Jusufi, N. Radacsi, A. A. Stokes, I. Park, M. Sitti, and M. Amjadi, "Wearable and stretchable strain sensors: Materials, sensing mechanisms, and applications," *Adv. Intell. Syst.*, vol. 2, no. 8, Aug. 2020, Art. no. 2000039.
[28] D. Ye, F. A. Panizzolo, C. Siviy, P. Malcolm, I. Galiana, K. G. Holt, and C. J. Walsh, "Effect of timing of hip extension assistance during loaded walking with a soft exosuit," *J. NeuroEng. Rehabil.*, vol. 13, no. 1, p. 87, 2016.
[29] A. R. Emmens, E. H. F. van Asseldonk, and H. van der Kooij, "Effects of a powered ankle-foot orthosis on perturbed standing balance," *J. NeuroEng. Rehabil.*, vol. 15, no. 1, p. 50, Dec. 2018.

[30] A. Martinez, B. Lawson, and M. Goldfarb, "Preliminary assessment of a lower-limb exoskeleton controller for guiding leg movement in overground walking," in *Proc. Int. Conf. Rehabil. Robot. (ICORR)*, Jul. 2017, pp. 375–380.

[31] G. Aguirre-Ollinger, A. Narayan, and H. Yu, "Phase-synchronized assistive torque control for the correction of kinematic anomalies in the gait cycle," *IEEE Trans. Neural Syst. Rehabil. Eng.*, vol. 27, no. 11, pp. 2305–2314, Nov. 2019.

[32] M. Hassan, H. Kadone, T. Ueno, Y. Hada, Y. Sankai, and K. Suzuki, "Feasibility of synergy-based exoskeleton robot control in hemiplegia," *IEEE Trans. Neural Syst. Rehabil. Eng.*, vol. 26, no. 6, pp. 1233–1242, Jun. 2018.

[33] J. S. Lora-Millan, J. C. Moreno, and E. Rocon, "Assessment of gait symmetry, torque interaction and muscular response due to the unilateral assistance provided by an active knee orthosis in healthy subjects," in *Proc. 8th IEEE RAS/EMBS Int. Conf. Biomed. Robot. Biomechatronics (BioRob)*, Nov. 2020, pp. 229–234.

[34] L. S. Vargas-Valencia, A. Elias, E. Rocon, T. Bastos-Filho, and A. Frizera, "An IMU-to-body alignment method applied to human gait analysis," *Sensors*, vol. 16, no. 12, p. 2090, Dec. 2016.

[35] J. A. Blaya and H. Herr, "Adaptive control of a variable-impedance ankle-foot orthosis to assist drop-foot gait," *IEEE Trans. Neural Syst. Rehabil. Eng.*, vol. 12, no. 1, pp. 24–31, Mar. 2004.

[36] H. Kawamoto and Y. Sankai, "Power assist method based on phase sequence and muscle force condition for HAL," *Adv. Robot.*, vol. 19, no. 7, pp. 717–734, 2005.

[37] J. Zhang, P. Fiers, K. A. Witte, R. W. Jackson, K. L. Poggensee, C. G. Atkeson, and S. H. Collins, "Human-in-the-loop optimization of exoskeleton assistance during walking," *Science*, vol. 356, no. 6344, pp. 1280–1284, Jun. 2017.

[38] L. N. Awad, J. Bae, K. O'Donnell, S. M. M. De Rossi, K. Hendron, L. H. Sloot, P. Kudzia, S. Allen, K. G. Holt, T. D. Ellis, and C. J. Walsh, "A soft robotic exosuit improves walking in patients after stroke," *Sci. Transl. Med.*, vol. 9, no. 400, pp. 1–13, Jul. 2017.

[39] H. F. Maqbool, M. A. B. Husman, M. I. Awad, A. Abouhossein, N. Iqbal, and A. A. Dehghani-Sanij, "A real-time gait event detection for lower limb prosthesis control and evaluation," *IEEE Trans. Neural Syst. Rehabil. Eng.*, vol. 25, no. 9, pp. 1500–1509, Sep. 2017.

[40] R. Ronsse, T. Lenzi, N. Vitiello, B. Koopman, E. Van Asseldonk, S. M. M. De Rossi, J. Van Den Kieboom, H. Van Der Kooij, M. C. Carrozza, and A. J. Ijspeert, "Oscillator-based assistance of cyclical movements: Model-based and model-free approaches," *Med. Biol. Eng. Comput.*, vol. 49, no. 10, pp. 1173–1185, 2011.

[41] F. Giovacchini, F. Vannetti, M. Fantozzi, M. Cempini, M. Cortese, A. Parri, T. Yan, D. Lefeber, and N. Vitiello, "A light-weight active orthosis for hip movement assistance," *Robot. Auton. Syst.*, vol. 73, pp. 123–134, Nov. 2015.

[42] S. Sahoo, M. Saboo, D. K. Pratihar, and S. Mukhopadhyay, "Real-time detection of actual and early gait events during level-ground and ramp walking," *IEEE Sensors J.*, vol. 20, no. 14, pp. 8128–8136, Jul. 2020.

[43] G. Panahandeh, N. Mohammadiha, A. Leijon, and P. Händel, "Continuous hidden Markov model for pedestrian activity classification and gait analysis," *IEEE Trans. Instrum. Meas.*, vol. 62, no. 5, pp. 1073–1083, May 2013.

[44] H. Prasanth, M. Caban, U. Keller, G. Courtine, A. Ijspeert, H. Vallery, and J. von Zitzewitz, "Wearable sensor-based real-time gait detection: A systematic review," *Sensors*, vol. 21, no. 8, p. 2727, Apr. 2021.

[45] A. F. Hidalgo, J. S. Lora-Millan, and E. Rocon, "IMU-based knee angle estimation using an extended Kalman filter," in *Proc. 41st Annu. Int. Conf. IEEE Eng. Med. Biol. Soc. (EMBC)*, Jul. 2019, pp. 570–573.

[46] Y.-L. Hsu, J.-S. Wang, Y.-C. Lin, S.-M. Chen, Y.-J. Tsai, C.-L. Chu, and C.-W. Chang, "A wearable inertial-sensing-based body sensor network for shoulder range of motion assessment," in *Proc. 1st Int. Conf. Orange Technol. (ICOT)*, Mar. 2013, pp. 328–331.

[47] C. M. N. Brigante, N. Abbate, A. Basile, A. C. Faulisi, and S. Sessa, "Towards miniaturization of a MEMS-based wearable motion capture system," *IEEE Trans. Ind. Electron.*, vol. 58, no. 8, pp. 3234–3241, Aug. 2011.

[48] T. Seel, T. Schauer, and J. Raisch, "Joint axis and position estimation from inertial measurement data by exploiting kinematic constraints," in *Proc. IEEE Int. Conf. Control Appl.*, Oct. 2012, pp. 45–49.

[49] S. L. Delp, F. C. Anderson, A. S. Arnold, P. Loan, A. Habib, C. T. John, E. Guendelman, and D. G. Thelen, "OpenSim: Open-source software to create and analyze dynamic simulations of movement," *IEEE Trans. Biomed. Eng.*, vol. 54, no. 11, pp. 1940–1950, Nov. 2007.

[50] A. Seth, J. L. Hicks, T. K. Uchida, A. Habib, C. L. Dembia, J. J. Dunne, C. F. Ong, M. S. DeMers, A. Rajagopal, M. Millard, S. R. Hamner, E. M. Arnold, J. R. Yong, S. K. Lakshmikanth, M. A. Sherman, J. P. Ku, and S. L. Delp, "OpenSim: Simulating musculoskeletal dynamics and neuromuscular control to study human and animal movement," *PLOS Comput. Biol.*, vol. 14, no. 7, Jul. 2018, Art. no. e1006223.

[51] A. Rajagopal, C. L. Dembia, M. S. DeMers, D. D. Delp, J. L. Hicks, and S. L. Delp, "Full-body musculoskeletal model for muscle-driven simulation of human gait," *IEEE Trans. Biomed. Eng.*, vol. 63, no. 10, pp. 2068–2079, Oct. 2016.

[52] E. F. Chehab, T. P. Andriacchi, and J. Favre, "Speed, age, sex, and body mass index provide a rigorous basis for comparing the kinematic and kinetic profiles of the lower extremity during walking," *J. Biomech.*, vol. 58, pp. 11–20, Jun. 2017.

[53] F. Moissenet, F. Leboeuf, and S. Armand, "Lower limb sagittal gait kinematics can be predicted based on walking speed, gender, age and BMI," *Sci. Rep.*, vol. 9, no. 1, pp. 1–12, Dec. 2019.

[54] N. C. Bejarano, E. Ambrosini, A. Pedrocchi, G. Ferrigno, M. Monticone, and S. Ferrante, "A novel adaptive, real-time algorithm to detect gait events from wearable sensors," *IEEE Trans. Neural Syst. Rehabil. Eng.*, vol. 23, no. 3, pp. 413–422, May 2015.

[55] R. Ronsse, S. M. M. D. Rossi, N. Vitiello, T. Lenzi, M. C. Carrozza, and A. J. Ijspeert, "Real-time estimate of velocity and acceleration of quasi-periodic signals using adaptive oscillators," *IEEE Trans. Robot.*, vol. 29, no. 3, pp. 783–791, Jun. 2013.

[56] W. van Dijk, C. Meijneke, and H. van der Kooij, "Evaluation of the Achilles ankle exoskeleton," *IEEE Trans. Neural Syst. Rehabil. Eng.*, vol. 25, no. 2, pp. 151–160, Feb. 2017.

[57] A. Findlow, J. Goulermas, C. Nester, D. Howard, and L. Kenney, "Predicting lower limb joint kinematics using wearable motion sensors," *Gait Posture*, vol. 28, no. 1, pp. 120–126, 2008.

[58] J. Y. Goulermas, A. H. Findlow, C. J. Nester, P. Liatsis, X. J. Zeng, L. P. Kenney, P. Tresadern, S. B. Thies, and D. Howard, "An instance-based algorithm with auxiliary similarity information for the estimation of gait kinematics from wearable sensors," *IEEE Trans. Neural Netw.*, vol. 19, no. 9, pp. 1574–1582, Sep. 2008.

[59] H. F. Maqbool, M. A. B. Husman, M. I. Awad, A. Abouhossein, N. Iqbal, M. Tahir, and A. A. Dehghani-Sanij, "Heuristic real-time detection of temporal gait events for lower limb amputees," *IEEE Sensors J.*, vol. 19, no. 8, pp. 3138–3148, Apr. 2019.

[60] M. Boutaayamou, M. A. B. Husman, M. I. Awad, A. Abouhossein, N. Iqbal, M. Tahir, and A. A. Dehghani-Sanij, "Development and validation of an accelerometer-based method for quantifying gait events," *Med. Eng. Phys.*, vol. 37, no. 2, pp. 226–232, 2015.

[61] B. Mariani, H. Rouhani, X. Crevoisier, and K. Aminian, "Quantitative estimation of foot-flat and stance phase of gait using foot-worn inertial sensors," *Gait posture*, vol. 37, no. 2, pp. 229–234, 2013.

[62] A. Mansfield and G. M. Lyons, "The use of accelerometry to detect heel contact events for use as a sensor in FES assisted walking," *Med. Eng. Phys.*, vol. 25, no. 10, pp. 879–885, 2003.

[63] A. Mannini, V. Genovese, and A. M. Sabatini, "Online decoding of hidden Markov models for gait event detection using foot-mounted gyroscopes," *IEEE J. Biomed. Heal. Informat.*, vol. 18, no. 4, pp. 1122–1130, Jul. 2014.

[64] J. Figueiredo, J. C. Moreno, and C. P. Santos, "Assistive locomotion strategies for active lower limb devices," in *Proc. ENBENG 5th Portuguese Meeting Bioeng.*, vol. 611695, Feb. 2017, pp. 1–4.

[65] C. Di Natali, G. Chini, M. Totaro, J. S. Lora-Millán, E. Rocon, L. Beccai, D. G. Caldwell, G. Visentin, and J. Ortiz, "Quasi-passive resistive exosuit for space activities: Proof of concept," *Appl. Sci.*, vol. 11, no. 8, p. 3576, Apr. 2021.

[66] V. Ruiz Garate, A. Parri, T. Yan, M. Munih, R. Molino Lova, N. Vitiello, and R. Ronsse, "Experimental validation of motor primitive-based control for leg exoskeletons during continuous multi-locomotion tasks," *Frontiers Neurorobot.*, vol. 11, p. 15, Mar. 2017.

[67] E. Zheng, S. Manca, T. Yan, A. Parri, N. Vitiello, and Q. Wang, "Gait phase estimation based on noncontact capacitive sensing and adaptive oscillators," *IEEE Trans. Biomed. Eng.*, vol. 64, no. 10, pp. 2419–2430, Oct. 2017.

[68] T. Yan, A. Parri, V. R. Garate, M. Cempini, R. Ronsse, and N. Vitiello, "An oscillator-based smooth real-time estimate of gait phase for wearable robotics," *Auton. Robots*, vol. 41, no. 3, pp. 759–774, May 2016.

[69] K. A. Hawkins, D. J. Clark, C. K. Balasubramanian, and E. J. Fox, ''Walking on uneven terrain in healthy adults and the implications for people after stroke,'' *NeuroRehabilitation*, vol. 41, no. 4, pp. 765–774, Dec. 2017.
[70] M. K. Holden, K. M. Gill, and M. R. Magliozzi, ''Gait assessment for neurologically impaired patients,'' *Phys. Therapy*, vol. 66, no. 10, pp. 1530–1539, Oct. 1986.

JULIO S. LORA-MILLAN was born in Cordoba, Spain, in 1991. He is currently pursuing the Ph.D. degree in automatic control and robotics with the Technical University of Madrid. In 2015, he finished his studies in automatics and industrial electronics engineering at the Universidad de Cordoba, being awarded the Exceptional Award for the Best Academic Record. In 2016, he joined the Centre for Automation and Robotics, Spanish National Research Council. In 2018, he was awarded with a Training Program for Academic Staff Contract by the Spanish Science, Innovation and Universities Ministry. His research interests include developing robotic and electronic systems to assist neurologically impaired subjects, especially their control algorithms and the interaction between users and devices.

ANDRES F. HIDALGO received the bachelor's degree in mechanical engineering from the Universidad Nacional de San Juan, Argentina, and the master's and Ph.D. degrees from the Polytechnic University of Madrid, Spain, in 2009 and 2013, respectively. He has worked in oil and gas and manufacturing industry for some years. After his Ph.D. degree, he worked as a Postdoctoral Researcher with the University of Seville and the Centre for Automation and Robotics CAR-CSIC, Spain. During the last years, he worked as a Simulation and Performance Engineer at Toyota Gazoo Racing Europe Team. In 2021, he started a new postdoctoral position at the Istituto Italiano di Tecnologia (IIT).

EDUARDO ROCON (Member, IEEE) was born in Vitoria, Brazil, in 1979. He received the degree in electrical engineering from the Universidade Federal do Espirí to Santo (UFES), in 2001, and the Ph.D. degree from the Universidad Politécnica de Madrid, in 2006. He is currently a Tenure Researcher with the Centre for Automation and Robotics, Spanish National Research Council. His research interests include rehabilitation, neurophysiology, biomechanics, adaptive signal processing, and human–machine interaction. His research activity was awarded with the Georges Giralt Ph.D. Award as the Best Ph.D. Robotics Thesis in Europe and the EMBEC Scientific Award.